SCIENTIFIC REPORTS

OPEN

SUBJECT AREAS:
OPTICAL PHYSICS
ATOMIC AND MOLECULAR PHYSICS
PLASMA PHYSICS
ULTRAFAST LASERS

Received
29 January 2014

Accepted
13 February 2014

Published
5 March 2014

Correspondence and requests for materials should be addressed to C.S. (christian.spielmann@uni-jena.de)

* Current address: Department of Physics, Lund University, PO Box 118, 22100 Lund, Sweden

Parametric amplification of attosecond pulse trains at 11 nm

J. Seres[1,2], E. Seres[1,2,3,4], B. Landgraf[1,4], B. Ecker[4,5], B. Aurand[4,5]*, A. Hoffmann[1], G. Winkler[2], S. Namba[6], T. Kuehl[4,5] & C. Spielmann[1,4]

[1]Institute of Optics and Quantum Electronics, Abbe Center of Photonics, Friedrich Schiller University, Max Wien Platz 1, 07743 Jena, Germany, [2]Institute of Atomic and Subatomic Physics, Vienna University of Technology, Stadionalle 2, 1020 Vienna, Austria, [3]Wolfgang Pauli Institute, CNRS UMI 2842, Nordbergstrasse 15, 1090 Vienna, Austria, [4]Helmholtz Institute Jena, Fröbelstieg 3, 07743 Jena, Germany, [5]GSI Helmholtz Centre for Heavy Ion Research, Planckstrasse 1, 64291 Darmstadt, Germany, [6]Graduate School of Engineering, Hiroshima University, 1-4-1 Kagamiyama, Higashi-Hiroshima, Hiroshima 739-8527, Japan.

We report the first experimental demonstration of the parametric amplification of attosecond pulse trains at around 11 nm. The helium amplifier is driven by intense laser pulses and seeded by high-order harmonics pulses generated in a neon gas jet. Our measurements suggest that amplification takes place only if the seed pulse-trains are perfectly synchronized in time with the driving laser field in the amplifier. Varying the delay, we estimate the durations of the individual extreme ultraviolet pulses within the train to be on the order of 0.2 fs. Our results demonstrate that strong-field parametric amplification can be a suitable tool to amplify weak attosecond pulses from non-destructive pump-probe experiments and it is an important step towards designing amplifiers for realization of energetic XUV pulses with sub-femtosecond duration using compact lasers fitting in university laboratories.

Intense short laser pulses focused in gases lead to the generation of femtosecond and even attosecond extreme ultraviolet (XUV) pulses via high-order harmonic generation (HHG)[1–6]. Moreover, the short wavelength pulses are not only temporally but also spatially coherent showing an exceptional high beam quality over a wide spectral range, making the sources suitable for wide range of x-ray spectroscopic applications. However, only a small fraction of the x-ray radiation is diffracted, transmitted or reflected by most samples, requiring intense input beams to achieve a sufficient signal to noise ratio. As the conversion efficiency for HHG is low, the x-ray pulse energy must be boosted up by an amplifier (Fig. 1(a)). However, powerful XUV beams can easily damage or degrade the sample to be studied[7]. Nondestructive measurements with low power XUV beams include spectroscopy of trapped individual molecules or nanoparticles[8] or imaging of biological specimens. To increase the signal to noise ratio or make detection possible at all, it will be necessary to enhance the XUV signal after the interaction in an all optical amplifier as shown in Fig. 1(b).

One possible solution is a plasma based amplifier (x-ray lasers). With them, high harmonic pulses have been successfully amplified at selected wavelengths matching atomic transitions[9–11]. Though, the widths of the atomic transitions limit the pulse duration to the picosecond and sub-picosecond range. Alternatively, x-ray parametric amplification has been successfully implemented to demonstrate enhancement with a self-seeded configuration[9,10] and the recent model of the process predicts broadband amplification suitable for few-femtosecond and sub-femtosecond pulses, however the experimental verification has been missing so far.

Here we report the first experimental demonstration of the parametric amplification of attosecond pulse trains at around 11 nm using an additional gas jet to generate and control the weak XUV seeding signal. Our measurements suggest that amplification takes place only, if the seed pulse-train is perfectly synchronized to the driving laser pulse in the amplifier as predicted theoretically[14]. Varying the delay with sub-10-as temporal resolution, we were able to resolve electric field evolution within the attosecond pulse train and estimated the duration of the individual XUV pulses within the train to be about 0.2 fs.

Results

Techniques for high harmonic yield enhancement. To enhance the yield of high-order harmonic generation (HHG), different methods have been realized in the last years by using two or multi-gas jet arrangements, namely quasi-phase matching (QPM)[15–17] and attosecond-pulse-train or vacuum ultraviolet (APT or VUV) enhanced HHG[18–24]. Our current approach is based on x-ray parametric amplification (XPA)[12,13], a high order difference

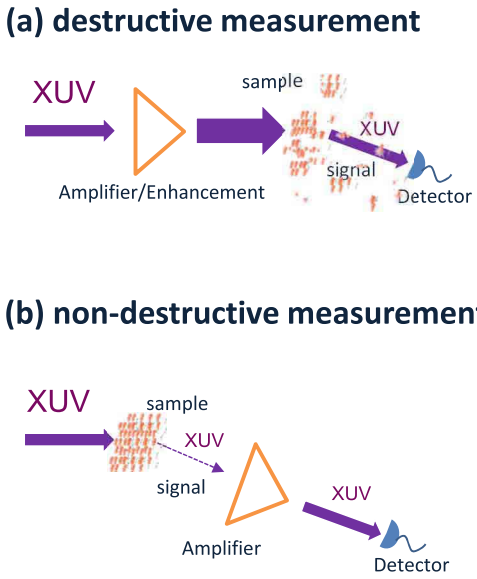

Figure 1 | X-ray measurement techniques. (a) Using a powerful XUV input beam ensures, even for very low interaction cross sections, a sufficient scattered or transmitted signal but the sample will be degraded or damaged. (b) Non-destructive experiments are based on a weak XUV input beam. The low signal after the interaction will be amplified to obtain a good signal to noise ratio for the detection.

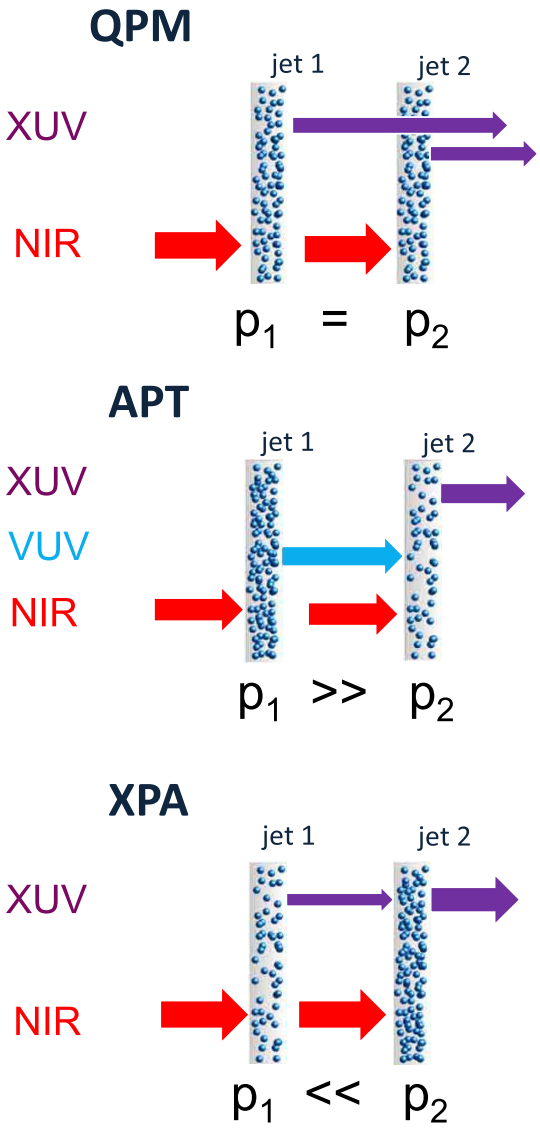

Figure 2 | Methods to enhance XUV radiation. In a two gas jet configuration the following schemes have been applied: quasi-phase matching (QPM), attosecond-pulse-train assisted (APT) enhancement, and x-ray parametric amplification (XPA). Experimentally the three approaches can be easily distinguished by the pressure p_1 and p_2 in the corresponding jets.

frequency generation process, which can be clearly distinguished from the other two methods. In Fig. 2, we provide an overview about the three different approaches, namely: **QPM:** Two (or more) gas jets are backed by the same gas with the same (or at least comparable) pressure. The fundamental laser beam generates high harmonics with the same spectrum and intensity in each gas jet. At a suitable jet distance and gas pressure, the two identical x-ray fields are added coherently, resulting in a factor of 4 (or N-squared if there are N jets[16,17]) enhancement of the on-axis intensity. **APT:** The first HHG source is optimized for producing intense VUV harmonics either below[18,23,24] or slightly above the ionization threshold of the gas used in the second source[18,20–22]. These requirements are best fulfilled by operating the first jet either at a high gas pressure[20,24] or having a long interaction length[21]. To assure an enhancement of the signal, either the gas pressure[20] or the ionization rate[21,22] must be kept at a low level in the second jet. **XPA:** The settings for XPA are opposite to APT, namely the gas pressure in the first HHG source is low to avoid on one hand a substantial modification of the transmitted laser pulse and on the other hand to generate only a weak XUV seed pulse for the second jet. In the second jet, both the pressure and the ionization rate must be as high as possible to realize large amplification via XPA. Further, in contrast to the other two techniques, only XPA is capable to amplify a signal originating from an independent source, e.g. a signal after the interaction with the sample in a spectroscopy experiment (Fig. 1(b)).

Experimental conditions. To demonstrate a HHG-seeded XUV amplifier based on XPA, our setup consists of two gas filled tubes (gas jets) backed with Ne and He respectively, as shown in Fig. 3(e). The 26-fs-long pulses of a Ti:sapphire laser system (see details in Method section) were focused to a peak intensity of 5×10^{15} W/cm^2 with a confocal parameter of 160 mm. In the first jet, a small fraction of the laser light is converted into a train of attosecond XUV pulses (see Fig. 3(c)). To investigate the characteristics of the He amplifier around 100 eV, we backed the first jet with low pressure Ne avoiding an alteration of the laser pulses. The HHG conversion efficiency for Ne is higher than for He, so even for rather low Ne pressure (few mbars) we are able to generate an XUV seed signal sufficient for saturating the He amplifier. At our experimental conditions, even using several favorable assumption (for details see Method section), the estimated harmonic output signal of the first jet is about four orders of magnitude too low for ionizing a substantial fraction of atoms in the second jet. So we can safely rule out QPM or APT/VUV enhanced HHG in our experiments.

At the quoted intensity, the corresponding cut-off photon energy[25] is several 100 eV. So at around 100 eV, the radiation can be generated over many optical cycles and by different long and short electron trajectories. Depending on various parameters, the kinetic energy of the electrons at the instant of recombination and consequently the frequency of the emitted radiation is slightly different. The measured spectrum (Fig. 3(a)) denotes the average over all these contributions and looks therefore more like a super-continuum than a line spectrum delivered in a spatially coherent beam with low divergence (Fig. 4(a)). The slightly perturbed fundamental laser pulse enters the second gas jet together with the XUV pulses. In the second jet, the electric field of the laser pulse ionizes atoms and accelerates the

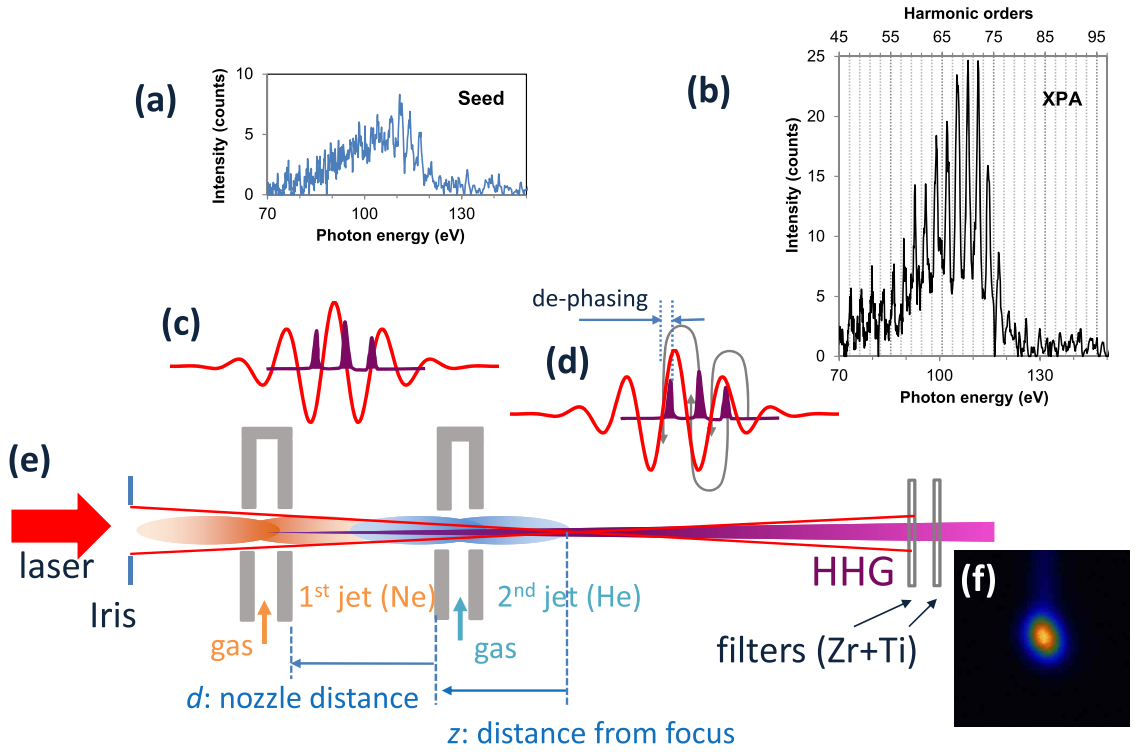

Figure 3 | Setup for x-ray parametric amplification and first measurements. (a) The broadband HHG spectrum is generated in the first jet, which (b) becomes a pronounced line spectrum after amplification in the second jet. (c) Attosecond pulses (violet) are generated in the first jet during every half optical cycle of the driving near-infrared laser pulse (red). (d) This pulse train is further amplified in the second jet if it arrives temporally synchronized with the re-colliding electrons (gray). (e) The experimental setup shows the collinear two-jet arrangement with the gas jets (gray) and the HHG beam (violet). (f) After blocking the fundamental laser radiation with thin metal filters (Zr-Ti) the beam profile was characterized with a CCD camera and the x-ray spectra were measured with a soft x-ray spectrograph.

released electrons during every half optical cycle[25] (Fig. 3(d), gray). Further amplification of the XUV pulses by XPA requires electrons moving along the so-called long trajectories[13]. Acceleration of these electrons takes somewhat longer so their return time to the ion is delayed compared to the electrons generating the seed HHG pulse train in the first jet[4,25]. Thus, the XUV pulses from the first jet arrive too early and cannot interact with the re-colliding electrons from the long trajectories in the second jet. Putting the two jets before the focus, an additional delay is introduced by the Gouy and atomic phase shift[13,25,26]. Choosing the distance of the jets properly, the de-phasing between the re-colliding electrons and the XUV pulse train can be compensated and amplification of the XUV pulse train takes place in the second jet, resulting in a well resolved harmonic line spectrum (Fig. 3(b)) with a small blue shift in agreement with the prediction for XPA in the high gain regime[13].

Beam profile narrowing. To study the effect of the temporal overlap, a series of beam profiles were measured for different separations d of the jets as shown in Fig. 4(a). The second (amplifier) jet was placed at a fixed position ($z_j = -15$ mm) before the laser focus and it was backed with He (backing pressure 4 bar). The first jet was backed with Ne (backing pressure 0.25 bar) and its separation from the second jet d has been varied. First, the beam profile of the amplifier jet was measured without any seed signal from the first jet by turning off the Ne gas supply. The very weak signal is termed as amplified spontaneous emission (ASE) and is just above the detection limit. Secondly, the seed beam profile was recorded without He gas supply for the amplifier jet. Finally, switching the gas in the amplifier jet on, the signal is enhanced, even for merged ($d = 0$ mm) jets, corresponding to non-optimized conditions. Increasing the distance between the two gas jets, the diameter and divergence of the XUV beam are reduced. The smallest far field beam diameters together with the strongest signals are observed for separations between 3 and 5 mm and the beams become slightly elliptical attributed to astigmatism introduced by the off-axis focusing of the laser beam with a spherical mirror. The smallest beam size is obtained for a distance of 4.3 mm, where the seed beam diameter (FWHM) of 4.5 ± 0.5 mm is reduced to 0.86 ± 0.10 mm. The beam profiles were measured 2.6 m from the source so we can estimate the divergence of the seed beam θ_{seed} and the amplified beam θ_{XPA} to 2.0 ± 0.3 mrad and 0.40 ± 0.03 mrad, respectively. The divergence decreases due to amplification in the following way[27]

$$\theta_{XPA}^{-2} \approx \theta_{seed}^{-2} + g_0 \theta_{amp}^{-2}. \quad (1)$$

From the measured ASE beam diameter of 2.3 ± 0.2 mm we can estimate the spatial acceptance angle for amplification θ_{amp} to 1.0 ± 0.1 mrad. They give a gain-length product of $g_0 = 6 \pm 2$ using Eq. (1).

Varying the distance between the jets. The fluence (see Method section) of the signal in the narrow central part of the beam (Fig. 4(a)) is plotted as a function of the jet distance in Fig. 4(b) and it shows a distinct maximum for a jet separation of 4.3 mm. The maximum signal implies the best temporal overlap between the XUV pulse train and the re-colliding electrons in the amplifier jet. Varying the jet distance affects the temporal overlap via the Gouy and atomic phase shift in the focused beam, as described in a recent paper[28]. We follow the logic of the paper and adapt it to our experimental condition.

In high harmonic generation, focused strong laser pulses with a peak intensity of I_0 interact with an atomic gas. The atomic phase (φ_{atom}) and the Gouy phase (φ_{Gouy}) in the focused beam cause a phase slip between the harmonic and fundamental laser beam. This phase slip depends on the position z of the jet (measured from

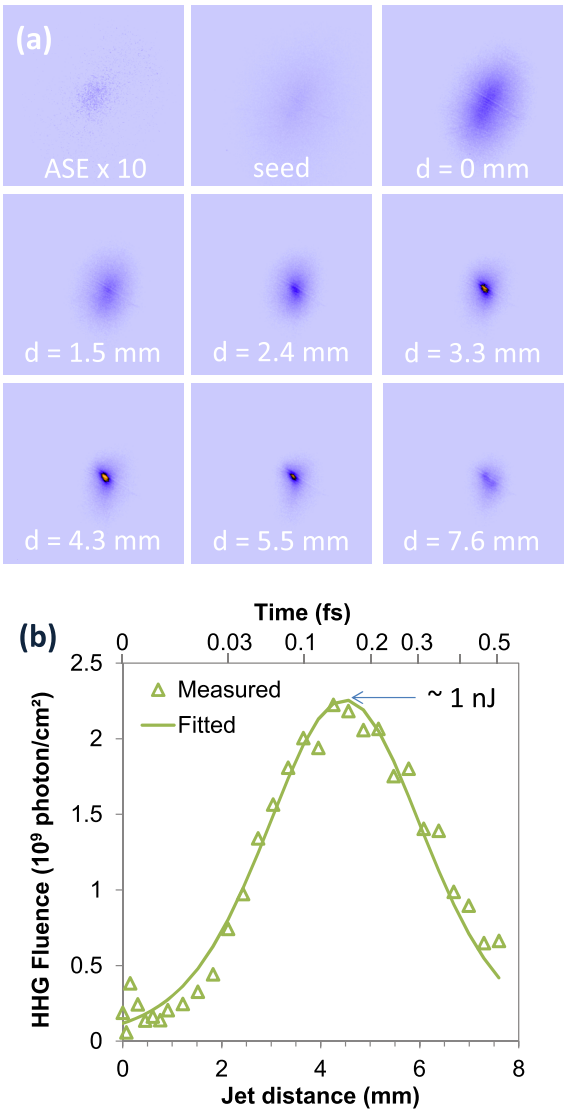

Figure 4 | Sub-femtosecond dynamics of the parametric amplification. (a) The beam profiles of the generated XUV beams have been measured with an x-ray CCD, namely the amplified spontaneous emission (ASE) from the helium amplifier jet without seed, the seed beam generated in the neon jet alone, and the beam profiles of the amplified XUV beam at around 110 eV were recorded for several jet distances. The gas backing pressures in the seed and amplifier jets were 0.25 bar and 4 bar for Ne and He, corresponding to about 6 mbar and 100 mbar real pressures in the interaction range, respectively. (b) The measured fluence of the amplified XUV signal reached a maximum at 4.3 mm jet distance. The distance is converted into a delay between the re-colliding electrons in the second jet and the XUV pulses generated in the first jet giving a 0.3 fs (FWHM) temporal window for amplification.

the focus position in the direction of laser propagation, see Fig. 3(e)) and is given by[26,13]

$$\varphi(z)=\frac{q\omega_1 z}{c}n_0\left(\delta-\frac{e^2 z}{2\varepsilon_0 m_e\omega_1^2}\right)+\alpha_q I_0\frac{z_R^2}{z^2+z_R^2}+qArctan\left(\frac{z}{z_R}\right). \quad (2)$$

Here q is the harmonic order, ω_1 is the angular frequency of fundamental laser beam, $1+\delta$ is the refractive index of the gas medium at the laser wavelength, n_0Z is the free electron density created by ionization, m_e is the mass of the electron, z_R is the Rayleigh length of the focused beam and parameter θ_q depends on the gas and electron trajectories (short or long). As outlined in Fig. 3(e), for two jets separated by a distance d and located at the positions $z = z_j$ and $z = z_j - d$, the magnitude of the phase between the two jets is dominated by the contributions of the last two terms of Eq. (2), because the gas density between the jets $n_0 \approx 0$. In Sec. III A of Ref. 13, the following condition for x-ray parametric amplification (XPA) is given

$$L\partial_z\left(\varphi_{atom}+\varphi_{Gouy}\right)=\Delta\varphi(z_j)\approx 0. \quad (3)$$

The derivatives in Eq. (3) can be calculated at the position $z = z_j$, and Eq. (3) is valid, if the length of the laser medium $L \ll z_R$, which is fulfilled in our experiments. To solve Eq. (3), we have to calculate the derivative on the left side

$$\Delta\varphi(z_j)=\frac{qLz_R}{z_j^2+z_R^2}\left[1-\frac{\alpha_q I_0}{q}\frac{2z_j z_R}{z_j^2+z_R^2}\right]\approx 0. \quad (4)$$

Eq. (4) is valid, if the factor in the brackets vanishes,

$$\frac{\alpha_q I_0}{q}=\frac{z_j^2+z_R^2}{2z_j z_R} \quad (5)$$

meaning that it is not necessary to know the correct value of α_q and I_0 when XPA is the main contributing process. Substituting Eq. (5) into Eq. (2) and assuming $n_0 \approx 0$ (almost no gas between the two jets), the phase difference between the two jets is given by the following equation

$$\begin{aligned}\Delta\varphi(d)=&q\frac{z_R}{2z_j}\frac{z_j^2+z_R^2}{(z_j-d)^2+z_R^2}-q\frac{z_R}{2z_j}\\&+qArctan\left(\frac{z_j-d}{z_R}\right)-qArctan\left(\frac{z_j}{z_R}\right).\end{aligned} \quad (6)$$

The temporal shift can be determined from the relation $\omega_1\tau = \Delta\varphi$ using the expression for the phase difference given in Eq. (6) and reads now

$$\tau=\frac{q}{\omega_1}\left[Arctan\left(\frac{z_j-d}{z_R}\right)-\frac{z_R}{2z_j}\frac{(z_j-d)^2}{(z_j-d)^2+z_R^2}\right]+\tau_0, \quad (7)$$

where τ_0 is an offset to ensure $\tau = 0$ for $d = 0$, $q = 73$ (11 nm), $z_j = -15$ mm and $z_R = 80$ mm. Using Eq. (7) with the experimental parameter above, the separation is converted into delay and added as second axis to Fig. 4(b). High fluence, i.e. a substantial gain, is only obtained near the optimum delay in the range between 0.05 and 0.35 fs (0.30 ± 0.05 fs, FWHM).

XPA as saturated amplifier. In another set of experiments we investigated how the gas pressure in the seed jet affects the XUV on-axis fluence with and without amplification, i.e. with the gas supply in the amplifier jet turned on and off, respectively. For a fixed jet distance of 3.3 mm, when the XPA beam diameter was the smallest, the beam profiles were measured similarly to Fig. 4(a). For the seed jet, we have estimated the atomic density n_0 and subsequently the free electron density $n_e = n_0Z$ from the known backing pressure (see Method section), where Z is the estimated degree of ionization. The measured output fluence as function of the estimated atomic density is plotted in Fig. 5(a). The seed fluence increases with the seed pressure or atomic density over the whole range of interest. More interestingly, the scaling of the XPA output fluence can be well modeled (blue dashed line in Fig. 5(a)) with the well-known formula describing the signal evolution of a saturated amplifier[29]

$$j=ln\left[1+G_0\left(e^{j_0}-1\right)\right], \quad (8)$$

where $j = J_{XPA}/J_{sat}$ is the output fluence J_{XPA} normalized to the saturation fluence J_{sat}; $j_0 = J_{Seed}/J_{sat}$ is the normalized input fluence

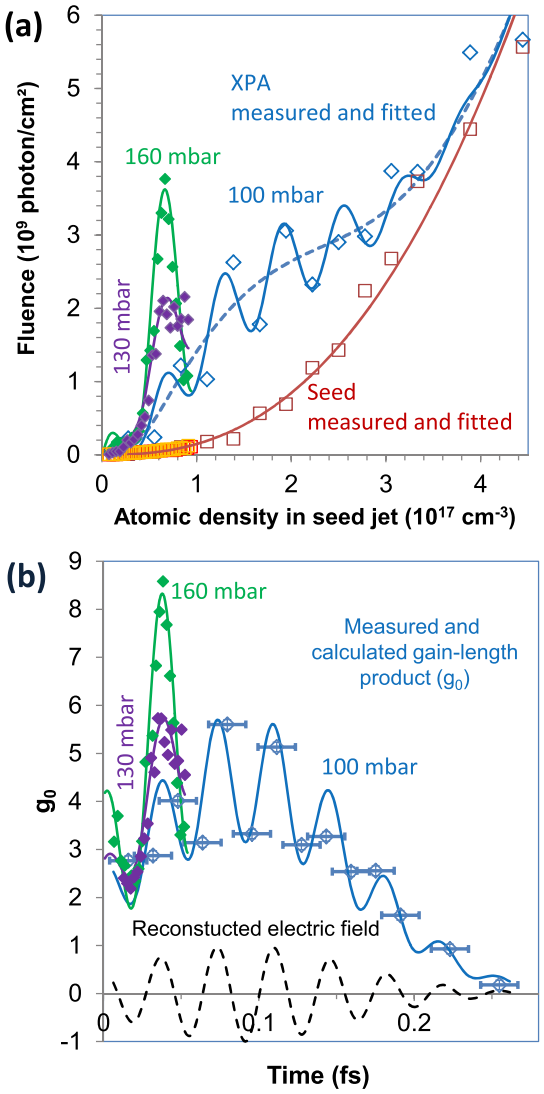

Figure 5 | Reconstruction of XUV pulses at 11 nm. (a) The measured XUV fluence without amplification (seed, brown curve) scales with the atomic density in the seed jet like a phase matched HHG source. Please note, the atomic density can be controlled with the backing pressure. The observed fluence with amplification behaves like a saturated amplifier (blue-violet-green) with periodically changing gain. (b) Deriving the gain from the measured data (blue-violet-green diamonds) as a function of the delay opens the possibility to reconstruct the average shape of the XUV pulses in the pulse train. Their electric field (dashed black) suggests pulse duration (FWHM) of about 0.2 fs.

J_{seed}; and $G_0 = e^{g_0}$ is the small signal or unsaturated gain, while the saturated gain can be calculated as $G = j/j_0$. When the amplifier is deeply saturated, ($J_{Seed} \gg J_{sat}$), Eq. (8) can be simplified and the output signal can be calculated as

$$J_{XPA} \approx g_0 J_{sat} + J_{Seed}. \tag{9}$$

Eq. (9) suggests that in the deep saturation regime, the output fluence of the amplifier is mainly determined by the seed fluence and is proportional to g_0. Furthermore, it is not possible to determine g_0 and J_{sat} independently. A determination is only possible by studying the scaling of n_e with the pressure in more detail.

Electric field reconstruction. The more detailed inspection reveals that the measured output signal (Fig. 5(a), blue diamonds) carries a sinusoidal modulation (Fig. 5(a), blue curve). The modulation has the same origin as the scaling of the output fluence with the jet distance. Not only the jet distance but also the free electron density in the seed jet modifies the delay between the seed attosecond pulse train and the re-colliding electrons in the amplifier jet. So, the delay can also be controlled very precisely by varying the gas pressure in the seed jet. Under typical experimental condition the dephasing $\Delta\varphi$ between the XUV and visible laser pulses is mainly governed by the plasma dispersion of the free electrons and can be calculated for a given jet length L, as

$$\Delta\varphi = \frac{e^2 n_e L}{2\varepsilon_0 m_e c \omega_1}, \tag{10}$$

with the free electron density n_e being proportional to the gas pressure and where ω_1 is the angular frequency of fundamental laser beam. As in the case of the jet distance consideration, the time delay $\tau = \Delta\varphi/\omega_1$ between the re-colliding electrons and x-ray pulses can be determined from the phase difference (Eq. (10)). If, in the second amplifier jet, the seed pulse train temporarily overlaps with the electron current of the re-colliding electrons, and furthermore the electric field of the XUV beam is in phase with the fundamental laser field (see Eq. (18) and Fig. 4 in Ref. 13), than the measured output signal and hence the gain is maximum. If the overlap is lost or the XUV electric field is out of phase, the signal enhancement will be negligible as described in a recent publication[14]. Summing up, the Gouy phase shift and the atomic phase shift significantly influence the magnitude of the gain, but the sinusoidal modulation observed in Fig. 5(a) is caused by the phase shift due to the changing density of free electrons. The gain g_0 as a function of the free electron density or time delay can be best fitted by assuming a Gaussian pulse envelope with a sinusoidal modulation (similar as in Ref. 14) and reads

$$g_0 = g_a \exp\left[-4ln2\frac{(\tau-\tau_0)^2}{\Delta\tau^2}\right][1 + V cos(\omega_1\tau)]. \tag{11}$$

V is the visibility of the periodic modulation, which is less than 1 due to the finite distribution of the re-colliding electrons and fluctuations of the free electron density considered by the error bars in Fig. 5(b) and is in good agreement with theoretical prediction[14]. To fit Eq. (11) to the experimental data, the magnitude of the free electron density in the seed jet and the real pressure in the amplifier jet has been obtained from an additional measurement as described in the Method section. For an estimated free electron density of 0.45% ± 0.01% of the atomic density given by the backing pressure, we can explain two experimental observations very well at the same time: First, the modulated curves as shown in Fig. 5(a) and 5(b) fit well to the measured data. Secondly, the periodicity of the gain plotted in Fig. 5(b) corresponds exactly to the period of the 11 nm XUV field. From the width and modulation depth ($V = 0.35$) we can reconstruct the average duration (FWHM) of the individual XUV pulses within the train to about 0.20 ± 0.05 fs as shown in Fig 5(b). The rather large error bars in Fig. 5(b), are mainly caused by the shot-to-shot instability of the driving laser and gas valve. It is also worth to mention, the varying free electron induced dephasing within the laser pulse is an additional source to smear out the pulses, preventing a full reconstruction of the exact electric field of the XUV pulses, so we can only approximate the electric field by a sinusoidal function. The fit also gives the average gain-length product of $g_a = 4.5$ and the maximum measured gain-length product is about 5.6, which is in the range of the previously predicted value obtained from the beam profile narrowing.

While the real He pressure in the amplifier jet was about 100 mbar in the previous measurement, two additional measurements were performed with increased He pressure, namely at about 130 mbar and 160 mbar. Furthermore, changing to a shorter jet length of about 2 mm and larger holes – tube diameter ratio allowed much higher

temporal resolution. With the improved parameters, within the applicable 0–1.2 bar backing pressure range, somewhat more than one optical period of the XUV pulses has been measured with high resolution as can be seen in Fig. 5(a) and 5(b) noted by green and violet diamonds (measurements) and fitted curves. At higher He pressures, proportionally higher gain-length product amplitudes of $g_a = 6.0$ and 7.2 were obtained from the fit and a maximal gain-length product as high as 8.7 has been achieved (Fig. 5(b)) giving an about four-time higher fluence and saturated gain of 60 (at 160 mbar He) compared to the previous about 15 (at 100 mbar He). Beyond the gain-length product, the measurements provided us with an estimate for saturated fluence of $J_{sat} = 0.5 \pm 0.1 \times 10^9 \frac{photon}{cm^2}$.

Discussion

In summary, with two subsequent gas jets backed with helium and neon, respectively, we have achieved amplification of attosecond-pulse-trains centered at around 11 nm. The same intense laser pulses generated the seed pulse-train in the first (neon) jet via conventional high harmonic generation and pumped the second (helium) amplifier gas jet. It has been shown that amplification is only made possible by precisely controlling the delay between the XUV pulses and the field of the driving laser pulses via the separation between the two jets or the gas pressure. More precisely, amplification takes place only over a delay range of 0.3 fs, from which we can estimate the width of XUV pulses to be about 0.2 fs. At optimum delay a maximum saturated amplification factor of up to 60 has been achieved. With the two-jet setup we will be able to generate XUV pulses having a higher brilliance due to the higher photon numbers, but also due to the substantially reduced divergence and beam diameter. Further, XPA requires orders of magnitude lower driving laser pulse energy compared to conventional plasma x-ray lasers, paving the way to realize powerful laser-driven XUV amplifiers at kHz[12] or even MHz[32] repetition rates.

Methods

Experimental setup. The setup for demonstrating the HHG-seeded XUV amplifier consisted of two gas filled tubes (gas jets) backed with Ne or He respectively, as shown in Fig. 3(e). The 26-fs-long pulses of the JETI Ti:sapphire laser system (FSU, Jena, Germany) centered around 800 nm were focused (f/100) with a spherical mirror (radius of curvature of 6 m). The pulse energy on target and the far field beam diameter was controlled with an adjustable iris before the focusing mirror to get the highest possible amplification factor in the amplifier jet without spoiling the beam profile. The intensity in the focus was fixed to 5×10^{15} W/cm^2 and the confocal parameter was on the order of 160 mm. The two gas targets were placed before the focus at a distance z measured from the focal point (see Fig. 3(e)). Both gas targets had an interaction length of 3 mm and were, in order to reduce the gas load, operated with a pulsed valve at 10 Hz, synchronized to the laser pulses. In the experiments we were able to adjust the longitudinal position of both jets independently, i.e. we controlled the position z of each jet and the distance d between them. The second (amplifier) jet was placed at a fixed position ($z = -15$ mm) before the laser focus to assure the optimal condition for XPA in every measurement and it was backed with He (backing pressure 4 bar). The first jet was backed with Ne (backing pressure between 0 and 1.2 bar) and its separation from the second jet d was varied. From beam profile measurement of the pump laser beam we determined the Rayleigh length $z_R = 80$ mm. After blocking the fundamental laser light with thin Zr (200 nm) and Ti (200 nm) foils, we measured either the far field beam profiles with a soft x-ray CCD camera (Andor iKon-L DO936N-BR-DD located 2.6 m downstream of the gas jet) or the spectra with an x-ray spectrograph (McPherson 248/310G) equipped with a 300 grooves/mm grating and a MCP detector.

Pulse fluence and energy measurement. To determine the energy of the x-ray pulses, we integrated the signal over the full beam profile as displayed on the CCD camera. For measuring the fluence we considered only the average of 5×5 pixels area at the intensity peak (N_c; count/pulse). The signals were multiplied with the gain (G = 15 e$^-$/count; given by the output node capacity of $\sim 1 \times 10^6$ e$^-$ and the 16-bit digitization depth) as found in the manual of the CCD camera (Andor iKon-L DO936N-BR-DD). Furthermore, the average energy required to create an e–h pair in the CCD is $\sim$3.65 eV/e$^-$, and the quantum efficiency at 110 eV is about QE = 0.01. From these data it is possible to calculate the detected pulse energy

$$W_{\det} \approx 3.65 \cdot e \cdot N_c \cdot G/QE \approx 8.8 \times 10^{-7} nJ/count \cdot N_c. \quad (12)$$

For the detected fluence, we have to normalize the measured signal by the area (13.5×13.5 μm^2) of a single pixel of the camera:

$$J_{\det} = \frac{3.65eV/e^- G}{110eV/photon \cdot (13.5\mu m)^2} N_c \approx 2.73 \cdot 10^5 \frac{photon}{count \cdot cm^2} \cdot N_c \quad (13)$$

To estimate the generated XUV pulse energy and fluence, we have to correct the measured numbers with transmission of the two 200-nm-thick Zr and 200-nm-thick Ti foils, which is in the order of 0.04, yielding

$$W_{gen} \approx 2.2 \cdot 10^{-5} nJ/count \cdot N_c \quad (14)$$

$$J_{gen} \approx 6.83 \cdot 10^6 \frac{photon}{count \cdot cm^2} \cdot N_c \quad (15)$$

Under optimized experimental conditions for highest fluence (4.3 mm jet distance, 250 mbar Ne and 4 bar He backing pressures) the amplified XUV pulse energy in the narrow (yellow) beam in Fig. 4(a) was about 1 nJ.

APT/VUV enhanced HHG. The ionization potential of Ne (21.6 eV) in the seed jet is somewhat smaller than for He (24.6 eV) in the amplifier jet. The slightly different ionization potential implies an about two-times lower ionization rate for He for the same laser intensity. At our experimental conditions we have ionized about 20% of the Ne and about 10% of the He atoms, respectively. To proof that the high harmonic radiation generated in the Ne-jet is not strong enough to ionize a substantial fraction of the He atoms, we estimated the atomic density in the interaction region. For this measurement, the first seed jet was backed with Ar and the pressure was chosen to maximize the XUV signal at about 40 nm (30 eV), where He is highly absorbing and the HHG signal decreases significantly after switching on the He jet.

From this measurement we are able to calculate the actual gas density in the He jet. The estimated density is about 2–4% of the value corresponding to the measured backing pressure, which is under control of the experimentalists. For this estimation it is not necessary to know the pressure distribution along the laser beam $p(z)$, because absorption is a linear process and an effective pressure p_{eff} can be used which is independent of the pressure distribution inside and outside of the jet:

$$p_{eff} = \frac{1}{L} \int_{-\infty}^{\infty} p(z) dz. \quad (16)$$

In most of the experiments, the measured backing pressure was 4 bar for He and 250 mbar for Ne, respectively. Both jets were identical, i.e. valves and nozzle shapes are the same, so the actual pressure in the interaction region is about 100 mbar He or 6 mbar Ne and about 10^{14} atoms were in the illuminated volume of the Ne jet.

The 11th and 15th harmonics are the lowest order harmonics to excite or ionize He atoms in the second jet. Even for these low order harmonics, the energy conversion efficiency has been always below 10^{-3} in Xe[30], and below 10^{-5} in Ne[31]. Consideringthe energy conversion efficiency and the higher photon energy of the harmonic signal, we expect for Ne 10^{10} VUV photons in a harmonic line for an incident laser pulse having 10^{16} photons in the interaction volume. In the amplifier jet, 10^{15} He atoms are in the illuminated volume and about 10% of them are ionized by the laser pulse, i.e. 10^{14} ionization events take place during every laser pulse. Every VUV photon from the first jet can assist ionization in the second jet. However, the maximum number of assisted ionization events will be given by the incident number of VUV photons and is limited to 10^{10} assisted ionization events out of 10^{14} laser field driven ionization events. Consequently, VUV assisted HHG will only contribute to a minor extent (less than 10^{-4}) to the signal, and is within the measurement error.

As demonstrated recently in a two jet configurations, the HHG signal is enhanced in the presence of VUV radiation having photon energies less than the ionization potential U_i. In these experiments, the additional lower energy photon $\hbar\omega_1$ contributes to the cutoff of the HHG photons $\hbar\omega_2$ in the following way:

$$\hbar\omega_2 = U_i + 3.17U_p + \hbar\omega_1 \quad (17)$$

where U_i and U_p are the ionization and ponderomotive potentials, respectively. With the additional photon present, harmonics should be observed above the cutoff given by the ponderomotive potential, or at least a strong enhancement of the signal near the cutoff. The observation of an extended cutoff has been described theoretically[19] and realized experimentally[22].

Another possibility to distinguish between HHG and VUV enhanced HHG is the following: In the second jet the pressure and/or ionization rate (due to the laser field alone) must be very low and in the first jet a powerful VUV beam must be generated by using either Xe or Ar[20,21,24] with a high pressure. As outlined above, the parameters in our experiments didn't meet these guidelines: In the first jet we used Ne at low pressure and in the second jet the pressure and ionization rate are rather

high. So we can safely claim that the enhancement in our setup is of different origin than the enhancement effects in those previous experiments.

1. Paul, P. M. *et al.* Observation of a Train of Attosecond Pulses from High Harmonic Generation. *Science* **292**, 1689–1692 (2001).
2. Hentschel, M. *et al.* Attosecond metrology. *Nature* **414**, 509–513 (2001).
3. Nabekawa, Y. *et al.* Conclusive Evidence of an Attosecond Pulse Train Observed with the Mode-Resolved Autocorrelation Technique. *Phys. Rew. Lett.* **96**, 083901 (2006).
4. Gallmann, L., Cirelli, C. & Keller, U. Attosecond Science: Recent Highlights and Future Trends. *Annu. Rev. Phys. Chem.* **63**, 447–469 (2012).
5. Sansone, G., Calegari, F. & Nisoli, M. Attosecond Technology and Science. *IEEE J. Sel. Top. Quant. Electr.* **18**, 507–519 (2012).
6. Goulielmakis, E. *et al.* Single-Cycle Nonlinear Optics. *Science* **320**, 1614–1617 (2008).
7. Gaffney, K. J. & Chapman, H. N. *et al.* Imaging Atomic Structure and Dynamics with Ultrafast X-ray Scattering. *Science* **316**, 1444–1448 (2007).
8. Marago, O. M., Jones, P. H., Gucciardi, P. G., Volpe, G. & Ferrari, A. C. Optical trapping and manipulation of nanostructures. *Nature Nanotech.* **8**, 807–819 (2013).
9. Zeitoun, Ph. *et al.* A high-intensity highly coherent soft X-ray femtosecond laser seeded by a high harmonic beam. *Nature* **431**, 426–429 (2004).
10. Wang, Y. *et al.* Phase-coherent, injection-seeded, table-top soft-X-ray lasers at 18.9 nm and 13.9 nm. *Nature Phot.* **2**, 94–98 (2008).
11. Hasegawa, N. *et al.* Frequency Filter of Seed X-ray by Use of X-ray Laser Medium: Toward the Generation of the Temporally Coherent X-ray Laser. *Jpn. J. Appl. Phys.* **48**, 012503 (2009).
12. Seres, J. *et al.* Laser driven amplification of soft-x-rays by parametric stimulated emission in neutral gases. *Nature Phys.* **6**, 455–461 (2010).
13. Seres, J., Seres, E. & Spielmann, C. Classical theory of strong-field parametric amplification of x-rays. *Phys. Rev. A* **86**, 013822 (2012).
14. Serrat, C. Coherent Extreme Ultraviolet Light Amplification by Strong-Field-Enhanced Forward Scattering. *Phys. Rev. Lett.* **111**, 133902 (2013).
15. Seres, J. *et al.* Coherent superposition of laser-driven soft-X-ray harmonics from successive sources. *Nature Phys.* **3**, 878–883 (2007).
16. Pirri, A., Corsi, C. & Bellini, M. Enhancing the yield of high-order harmonics with an array of gas jets. *Phys. Rev. A* **78**, 011801(R) (2008).
17. Willner, A. *et al.* Coherent spectral enhancement of carrier-envelope-phase stable continua with dual-gas high harmonic generation. *Opt. Lett.* **37**, 3672–3674 (2012).
18. Ishikawa, K. Photoemission and Ionization of He^+ under Simultaneous Irradiation of Fundamental Laser and High-Order Harmonic Pulses. *Phys. Rev. Lett.* **91**, 043002 (2003).
19. Fleischer, A. Generation of higher-order harmonics upon the addition of high-frequency XUV radiation to IR radiation: Generalization of the three-step model. *Phys. Rev. A* **78**, 053413 (2008).
20. Gademann, G. *et al.* Attosecond control of electron–ion recollision in high harmonic generation. *New J. Phys.* **13**, 033002 (2011).
21. Heinrich, A. *et al.* Enhanced VUV-assisted high harmonic generation. *J. Phys. B* **39**, S275–S281 (2006).
22. Takahashi, E. J., Kanai, T., Ishikawa, K. L., Nabekawa, Y. & Midorikawa, K. Dramatic Enhancement of High-Order Harmonic Generation. *Phys. Rev. Lett.* **99**, 053904 (2007).
23. Ranitovic, P. *et al.* Controlling the XUV Transparency of Helium Using Two-Pathway Quantum Interference. *Phys. Rev. Lett.* **106**, 193008 (2011).
24. Brizuela, F. *et al.* Efficient high-order harmonic generation boosted by below-threshold harmonics. *Sci. Rep.* **3**, 1410 (2013).
25. Kohler, M. C., Pfeifer, T., Hatsagortsyan, K. Z. & Keitel, C. H. Frontiers of Atomic High-Harmonic Generation. *Advances in Atomic, Molecular, and Optical Physics* **61**, 159–207 (2012).
26. He, X. *et al.* Spatial and spectral properties of the high-order harmonic emission in argon for seeding applications. *Phys. Rev. A* **79**, 063829 (2009).
27. Stuart, B. C., Herman, S. & Perry, M. D. Chirped-Pulse Amplification in Ti:Sapphire Beyond 1 μm. *IEEE J. Quant. Electr.* **31**, 528–538 (1995).
28. Laban, D. E. *et al.* Extreme Ultraviolet Interferometer Using High-Order Harmonic Generation from Successive Sources. *Phys. Rev. Lett.* **109**, 263902 (2012).
29. Stuart, B. C., Herman, S. & Perry, M. D. Chirped-Pulse Amplification in Ti:Sapphire Beyond 1 μm. *IEEE J. Quant. Electr.* **31**, 528–538 (1995).
30. Takahashi, E., Nabekawa, Y. & Midorikawa, K. Generation of 10-μJ coherent extreme-ultraviolet light by use of high-order harmonics. *Opt. Lett.* **27**, 1920–1922 (2002).
31. L'Huillier, A. & Balcou, Ph. High-Order Harmonic Generation in Rare Gases with a 1-ps 1053-nm Laser. *Phys. Rev. Lett.* **70**, 774–777 (1993).
32. Seres, E., Seres, J. & Spielmann, C. Extreme ultraviolet light source based on intracavity high harmonic generation in a mode locked Ti:sapphire oscillator with 9.4 MHz repetition rate. *Opt. Express* **20**, 6185–6190 (2012).

Acknowledgments

This study has been sponsored by the DFG grant TR18 P12, SE 1911/1-1, and TMBWK grant B715-08008 and the European Fund for Regional Development (EFRE). E.S., J.S. and G.W. acknowledge support of Prof. Schumm. The authors acknowledge the support by Laserlab-Europe, project HIJ-FSU0019152 and the contributions of the JETI laser team.

Author contributions

J.S., E.S., S.N., T.K. and C.S. designed the experiments and wrote the manuscript; J.S., E.S., B.L., B.E., B.A., A.H., G.W. and S.N. carried out the experiments; all authors analyzed the data and contributed to the completion of the manuscript.

Additional information

Competing financial interests: The authors declare no competing financial interests.

How to cite this article: Seres, J. *et al.* Parametric amplification of attosecond pulse trains at 11 nm. *Sci. Rep.* **4**, 4254; DOI:10.1038/srep04254 (2014).